Effect of member grouping and pool size of discrete cross-sections on the optimal design of a large-scale 3D steel frame

Bethany M. Turay, bturay@clarkson.edu, Smith College, Northampton, MA, USA
Pedro L. Fernández-Cabán*, pfernand@clarkson.edu, Clarkson University, Potsdam, NY, USA
Kyle J. Thomson, thomso@clarkson.edu, Clarkson University, Potsdam, NY, USA

****Correspondence***

Keywords: steel frames; multi-story buildings; large-scale; discrete optimization; sizing optimization; member grouping; particle swarm; big bang-big crunch algorithm

Abstract

This paper examines the effect of member grouping and selected pool size of discrete cross-sections on the optimal design of a large-scale steel frame structure. Member grouping is commonly applied to structural optimization problems to significantly reduce the solution space of candidate designs and improve the efficiency and robustness of the search to achieve near-optimum solutions. At the same time, discrete sets of cross-sectional steel shapes (profile lists) assigned to a particular member group are often limited to a subset of cross-sections to further limit the search space and ensure practicality in the final design. However, for large-scale structural systems (e.g., tall buildings), limiting the number of member groups coupled with the exclusion of lighter cross-sectional shapes may significantly impact the quality of the optimal solution (i.e., weight of the frame). This work presents a case study of a large-scale three-dimensional (3D) steel frame to evaluate the sensitivity of the optimal design to practical combinations of member groups and steel profile lists used in multi-story steel frames. A recently developed metaheuristic search algorithm was applied to the steel frame and independent optimization experiments were performed for 16 unique member grouping and profile list combinations (cases) to quantify their influence on the variability and quality of the optimal design. Results reveal a 33% difference in the optimal (final) weight between member group and profile list combinations producing the smallest and largest solution spaces. Yet, the lightest design (corresponding to the largest solution space) produced a greater number of unique steel shapes and required significantly higher computational cost.

1 Introduction

Discrete member sizing optimization of civil engineering structures is a well-accepted approach for automating the design process to minimize material cost while meeting code-based (or user-based) performance demands related to the survivability, serviceability, and constructability of the structural system. Discrete sizing optimization entails selecting the lightest cross-sectional section from a discrete set (i.e., list) of structural shapes (e.g., W-Shapes). From a structural optimization standpoint, it is often desirable to limit the number of available shapes down to a subset of cross-sections to reduce the size of the design space (Barbosa et al., 2008; Lemonge et al., 2011; Carvalho et al., 2018; Peng et al., 2021) and improve the efficiency of the structural optimization algorithm. For the most part, the reduction of the design domain is, at least in part, performed based on prior knowledge regarding the behavior of the structural system (e.g., identifying structural members undergoing elevated internal forces). However, for large and complex structural systems (e.g., tall buildings), the exclusion of lighter cross-sectional shapes may significantly impact the quality of the optimal solution (i.e., weight of the frame).

The effect of limiting the set of available cross-sections is magnified when structural members are grouped together during the structural optimization process, which is readily implemented in literature to reduce the number of design variables in the optimization problem (e.g., Chan and Grierson, 1993; Chan and Chui, 2006; Walls and Elvin, 2010b; Spence and Kareem, 2014). In this case, selecting a heavier section for one member will affect all the members in the group. When performing member sizing on real-size multi-story framed structures, it is common practice to establish member groups according to their spatial orientation (e.g., vertical, horizontal, or diagonal members) and/or relative location within the structure. For instance, corner columns of consecutive stories may be grouped together to constitute one member group, while all beams supporting a particular floor may be grouped to have the same cross-section. Limiting the number of member groups helps reduce the search space of possible designs and, at the same time, often simplifies the fabrication process and constructability of the structural system. However, reducing the number of member groups may lead to heavier designs. For example, the structural capacity (e.g., load-to-capacity ratio) of a particular member group will be controlled by only a

few members experiencing the highest internal stresses in the group, while other members may be under-stressed. Therefore, strategically selecting the number of member groups (i.e., design variables) coupled with careful restriction of the pool size of available structural steel sections can have a significant impact on the quality of the optimization results. Yet, most studies on discrete sizing optimization of large-scale steel frames only consider a single member grouping arrangement and profile list of steel shapes (e.g., Hasançebi et al., 2011; Kaveh and Bolandgerami, 2017; Kaveh, 2021).

The main objective of this study is to offer a detailed examination of member grouping effects and the impact of limiting the set of available steel shapes (i.e., profile list) on a large-scale three-dimensional (3D) steel frame structure. A series of independent optimization experiments were performed on a 20-story steel frame for 16 combinations of member grouping and steel profile list arrangements. The work applied a recently developed hybridized particle swarm optimization (PSO) and the big bang-big crunch (BB-BC) algorithm equipped with a discrete stochastic search scheme, which was specifically calibrated for optimizing large-scale steel frames (Fernández-Cabán and Masters, 2018). The frame consisted of 1040 structural members. Due to the large size of the frame and the vast domain of possible designs (i.e., search space), the work leveraged the Accelerating Computational Research for Engineering and Science (ACRES) high-performance computing (HPC) cluster at Clarkson University and parallel processing to maintain the rigor of the search while significantly minimizing computational time. A detailed comparison of the optimal design found for different member grouping and profile list configurations along with statistical measures of the variability of the results is reported and discussed. Finally, conclusions and future research opportunities are highlighted.

2 Background

One of the main challenges of metaheuristics and population-based algorithms when applied to the design optimization of large-scale civil structures is performing a robust and efficient search of the vast domain of candidate designs and arrive at near-optimal solutions in a reasonable amount of computational time (Saka and Geem, 2013; Azad, 2021; Kaveh, 2021; Kashani et al., 2021). When sizing the structural members of real-world framed structures, the size of the (discrete) solution space can be

dramatically reduced by collecting structural members into groups (i.e., limiting the number of design variables) or bounding the discrete set of available structural shapes to only a subset of cross-sections. Figure 1 shows a schematic of a typical member grouping arrangement adopted in the optimization of multi-story 3D steel frames, where the structural members are collected into nd total groups and a unique set of discrete steel shapes ($Nsec$) are assigned to different types of structural members.

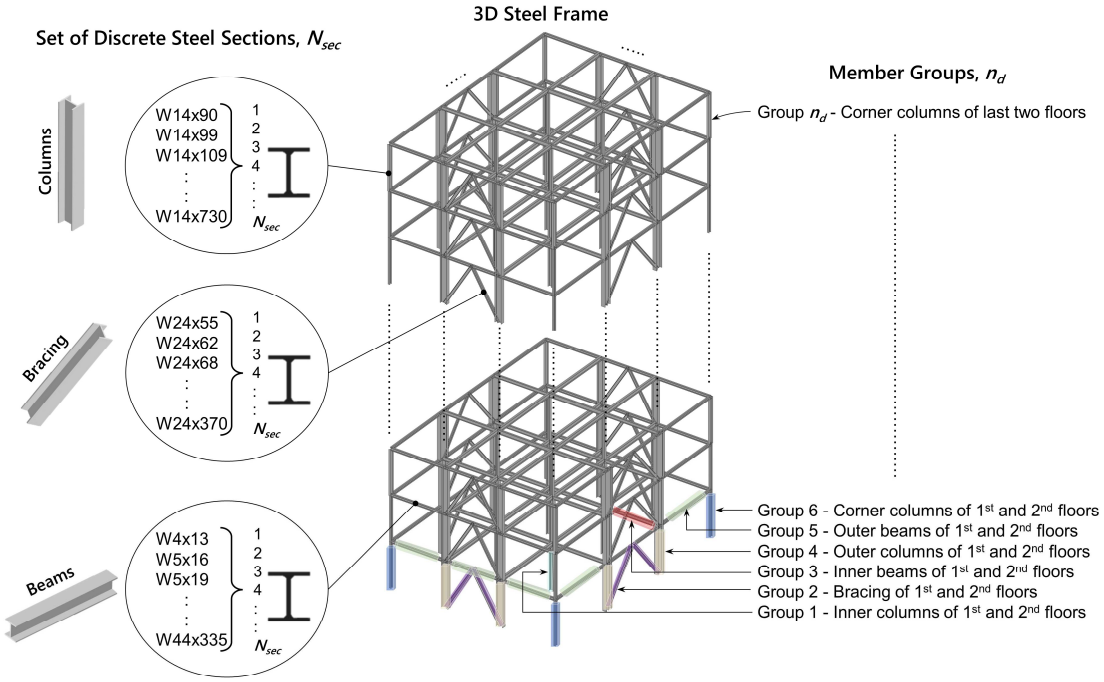

Figure 1. Illustration of member grouping and discrete set of available steel sections for a 3D multi-story steel frame.

The number of possible candidate designs (i.e., size of search space) as a function of nd and N_{sec} is illustrated in Figure 2. The surface plot was created assuming that each member group can select from a list of N_{sec} discrete steel shapes. For instance, the American Institute of Steel Construction (AISC) manual (2016) lists 297 distinct wide (W) flange sections. If all member groups can select from any of these W-shapes, then the size of the search space would be 297^{nd}. Increasing the search space can be desirable to improve the quality of the solution and potentially achieve a significantly lighter structural

system—i.e., assuming the optimization algorithm is robust enough and is not prone to getting trapped in a local optimum when applied to large-scale problems (Kaveh, 2021). At the same time, a larger search space could lead to a greater number of unique steel profiles and result in a more impractical and expensive design and increased complexity during construction (Barbosa et al., 2008; Lemonge et al., 2011; Boscardin et al., 2019). Therefore, arriving at optimal member grouping arrangements to reduce the overall cost of the structural systems is a non-trivial process, especially for large and complex structural systems.

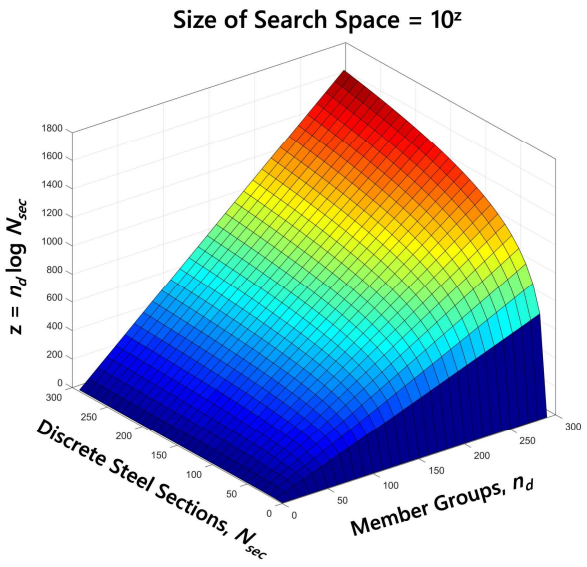

Figure 2. Size of solution space as a function of total number of member groups (nd) and profile list of available discrete steel sections (N_{sec}).

Previous studies have addressed the important role member grouping plays in the optimal design (e.g., cost) of civil structures. Grierson and Cameron (1987) developed a computer program called Structural Optimization Design & Analysis (SODA) for the automatic member sizing of steel frames. The software incorporated member groupings where the user was able to critique the final design and apply engineering judgment and heuristics to make changes to the design. Biedermann and Grierson (1995) subsequently introduced a Genetic Algorithm (GA) coupled to SODA to automate the design of building structures and later applied a neural network and heuristic design knowledge to achieve desirable member groupings of steel frame structures (Biedermann, 1997; Biedermann and Grierson, 1996).

Most of the literature regarding member grouping has primarily focused on pin-connected (i.e., trussed) structures (e.g., Galante, 1996; Barbosa et al., 2008; Toğan and Daloğlu, 2008). For example, Galante (1996) developed a multi-objective GA and Shea et al. (1997) proposed a shape annealing method with dynamic member grouping for the optimal design of trussed structures. More recently, Barbosa and Lemonge (2005) proposed a GA encoding to automatically satisfy a class of cardinality constraints, where the algorithm provided the designer with the possibility of directly controlling only the number of discrete cross-sectional shapes to be used in each problem and letting the GA search derive the grouping of the members. Cardinality constraints were successfully applied in future works to multiple benchmark truss problems considering sizing and shape/sizing optimization (Barbosa et al., 2008; Lemonge et al., 2010).

Few studies can be found in literature concerning the optimal member grouping for steel frame structures. Notable studies include the work of Walls and Elvin (2010a), which presented an automated algorithm for optimizing the grouping of discrete structural members of two-dimensional structures carrying axial and/or bending forces. The algorithm grouped members based on their mass per unit length and performed an exhaustive search of permutations to find the optimal arrangement of member groups. Lemonge et al. (2011) adopted a GA encoder approach originally used in pin-connected structures (Barbosa et al., 2008; Lemonge et al., 2010) that enforced cardinality constraint to search for the optimal member group arrangement of planar frames while grouping beams and columns independently. The current study expands on previous work by systematically examining the effect of selecting member groups and pool size of discrete steel sections commonly used in the design of large-scale three-dimensional (3D) steel frames on the optimal design.

3 Discrete member sizing optimization of 3D steel frames

The discrete member sizing optimization problem for the design of large-scale multi-story 3D steel frames consists of finding the optimal discrete set of cross-sectional shapes that will minimize the weight of the frame with a given topology. In this study, the optimal set of optimal steel shapes are selected from a list of standard wide-flange (W) shape sections tabulated in the American Institute of Steel Construction

(AISC) manual (2016). The optimization problem is constrained by multiple code-based (e.g., strength and drift limit states) to ensure that the optimal design provides adequate lateral stiffness to the system and user-specified constraints to satisfy constructability requirements. Strength checks of the structural members were performed using Load and Resistance Factor Design (LRFD) specifications from AISC (2016). Mathematically, the optimization problem can be formulated as follows:

Find

$$\mathbf{x} = [x_{i=1}, x_2, \dots, x_{nd}] \tag{1}$$

to minimize

$$W(\mathbf{x}) = \sum_{m=1}^{nm} \rho_m A_m L_m \tag{2}$$

subject to

$$g_m^{LCR}(\mathbf{x}) = LCR_m - 1 \leq 0 \qquad m = 1,2, \dots, nm \tag{3}$$

$$g_k^{ID}(\mathbf{x}) = ID_k - 1 \leq 0 \qquad k = 1,2, \dots, ns \tag{4}$$

$$g_j^{G}(\mathbf{x}) = G_j - 1 \leq 0 \qquad j = 1,2, \dots, nj \tag{5}$$

$$1 \leq x_i \leq N_{sec,i} \qquad i = 1,2, \dots, nd \tag{6}$$

where $\mathbf{x}$ is a vector of integers representing the sequence numbers of standard steel (W-Shape) sections assigned to nd design variables (i.e., member groups). $W(\mathbf{x})$ is the weight of the frame; ρ_m and A_m are the density and cross-sectional area of member m, respectively; L_m is the length of member m and nm is the total number of members; Eq. (6) constrains the bounds of each design variable entry x_i; $N_{sec,i}$ is the total number of standard steel sections in member group i. Eq. (3) and (4) represent inequality constraints for strength (Eq. 3) and serviceability (Eq. 4) requirements based on AISC-LRFD specifications (2016), while Eq. (5) represent geometric constraints to ensure all the connections between beam and column members are feasible. In Eq. (3), LCR_m is the load-capacity ratio defined as:

$$LCR = \begin{cases} \dfrac{P_u}{\phi P_n} + \dfrac{8}{9}\left(\dfrac{M_{ux}}{\phi_b M_{nx}} + \dfrac{M_{uy}}{\phi_b M_{ny}}\right) & \text{if } \dfrac{P_u}{\phi P_n} \geq 0.2 \\ \dfrac{P_u}{2\phi P_n} + \left(\dfrac{M_{ux}}{\phi_b M_{nx}} + \dfrac{M_{uy}}{\phi_b M_{ny}}\right) & \text{if } \dfrac{P_u}{\phi P_n} < 0.2 \end{cases} \quad (7)$$

where P_u is the required axial strength (i.e., tension or compression), M_{ux} and M_{uy} are the required flexural strength for strong and weak axis bending, respectively; P_n is the available axial strength; M_{nx} and M_{ny} are the available flexural strength for strong and weak axis bending, respectively; ϕ_b is the resistance factor for bending equal to 0.90; ϕ is the axial resistance factor, which equals 0.90 for compression and tensile yielding strength limit states.

Eq. (4) defines the inequality constraint for inter-story drift requirement of multi-story buildings, where ID_k can be expressed as follows:

$$ID_k = \frac{\delta_k - \delta_{k-1}}{\delta_{allw}} \qquad k = 1, \dots, ns \quad (8)$$

where $\delta_k - \delta_{k-1}$ is the relative lateral displacement of adjacent stories; δ_{allw} is the allowable interstory drift limit; ns is the total number of stories. In studies involving 3D frame structures, Eq (8) is typically applied to the orthogonal x and y horizontal building directions.

In addition to strength and drift constraints, geometric constraints were imposed on the optimization problem to ensure the optimal design achieves feasible beam-column connections. In Eq. (5), $G_j = G_{j,1} + G_{j,2}$, where:

$$G_{j,1} = \frac{b_{fb}}{b_{fk}} \qquad j = 1,2, \dots, nj \quad (9)$$

$$G_{j,2} = \frac{b'_{fb}}{d_c - 2t_f} \qquad j = 1,2, \dots, nj \quad (10)$$

The dimensional parameters presented in Eqs. (9) and (10) are depicted in Figure 3, in which b_{fb}, b'_{fb}, and b_{fk} are the flange width for beam 1 (B1), beam 2 (B2), and the column member, respectively; d_c and t_f are the depth and flange thickness of the column member, respectively. Eq. (9) ensures the flange width of beam B1 does not exceed the flange width of the column, while Eq. (10) enforces the flange

width of beam B2 to not exceed the difference between the depth of the column and the flange width of both sides of the column.

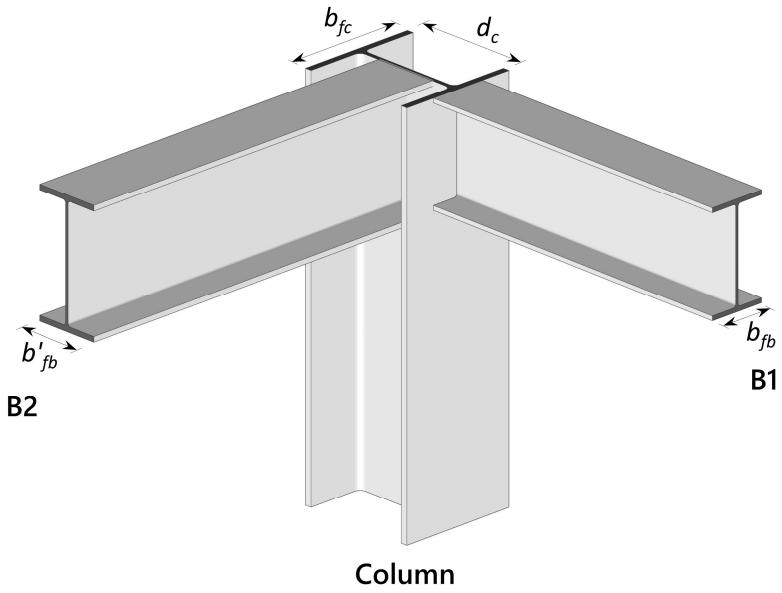

Figure 3. Schematic of dimensional parameters used for the geometric constraints of beam-column connections.

A penalty function approach (Azad and Hasançebi, 2015; Fernández-Cabán and Masters, 2018; Azad, 2021) is applied to transform the constrained optimization problem presented in Eqs. (1) – (6) into an unconstrained one:

$$\psi(\mathbf{x}, p) = W(\mathbf{x})[1 + pC(\mathbf{x})] \tag{11}$$

where p is a penalty coefficient (for this study, p = 0.1), and $C(\mathbf{x})$ is the penalty function defined as

$$C(\mathbf{x}) = \max[0, g(\mathbf{x})] \tag{12}$$

$$g(\mathbf{x}) = \sum_{m=1}^{nm} g_m^{LCR}(\mathbf{x}) + \sum_{k=1}^{ns} g_k^{ID}(\mathbf{x}) + \sum_{j=1}^{nj} g_j^{G}(\mathbf{x}) \tag{13}$$

4 Optimization algorithm

This study employs a recently developed explore-then-exploit (ETE) metaheuristic optimization strategy (Fernández-Cabán and Masters, 2018). The algorithm hybridizes two well-established metaheuristic strategies, namely particle swarm optimization (PSO) and big bang-big crunch (BB-BC). PSO is a metaheuristic technique which mimics the social behavior of organisms such as bird flocking and fish schooling (Kennedy and Eberhart, 1995) and has proven effective in the global investigation (i.e., exploration) of large design domains. The BB-BC algorithm was originally developed by Erol and Eskin (2006) and was inspired by one of the theories of evolution of the universe. Since then, improved, and hybridized versions of the original BB-BC algorithm have been developed and effectively applied to optimize civil engineering structures (e.g., Camp, 2007; Kaveh and Talatahari, 2010; Hasançebi and Azad, 2014). In this study, the ETE updating scheme used for the generation of new candidate designs follows:

$$\mathbf{x}_i^{k+1} = \text{round}\left[\theta_k \mathbf{G}^k + (1-\theta_k)\mathbf{P}_i^k\right] + \mathbf{d}_i \quad \text{for} \quad i = 1, \dots, N \tag{14}$$

where $\mathbf{x}_i^{k+1}$ is the position vector of particle i at iteration $k+1$; $\mathbf{G}^k$ is the position of the best solution found among all candidates up to iteration k (i.e., global best); $\mathbf{P}_i^k$ is the best position found by particle i up to iteration k (i.e., particle best); θ_k is a control parameter that linearly increases over a user-specified number of generations to control the relative influence of $\mathbf{P}_i^k$ and $\mathbf{G}^k$; $\mathbf{d}_i$ is a normal distribution operator from the BB-BC algorithm (Erol and Eksin, 2006). In this study, $\mathbf{d}_i$ is defined as:

$$\mathbf{d}_i = \text{round}\left[\alpha \mathbf{r}_i^n \left(\frac{\mathbf{x}_{max} - \mathbf{x}_{min}}{k}\right)\right] \quad i = 1, \dots, N \tag{15}$$

where $\mathbf{r}_i$ is a random number from a standard normal distribution; α is a parameter for controlling the size of the search space; n is an exponential parameter; $\mathbf{x}_{max}$ and $\mathbf{x}_{min}$ are the position vectors of the upper and lower bounds of each design variable, respectively. After each iteration, θ_k is adjusted to increase the influence of the global best solution ($\mathbf{G}^k$) on the swarm, thus effecting a gradual transition from exploration to exploitation of the search space. In this study, $\theta_k$is linearly increased after each iteration k following:

$$\theta_k = \left(\frac{\theta_f - \theta_i}{\beta k_{max} - 1}\right)(k-1) + \theta_i \tag{16}$$

where k_{max} is the maximum number of iterations; β is a parameter which defines the iteration when θ_k will transition from a linear variation to a final constant value; θ_i and θ_f are the initial and final values, respectively. The rounding function included in Eqs. (14) and (15) converts the continuous design variable into discrete integers representing a particular steel cross-section in the profile list of W-Shapes. A flowchart of the ETE algorithm is illustrated in Figure 4.

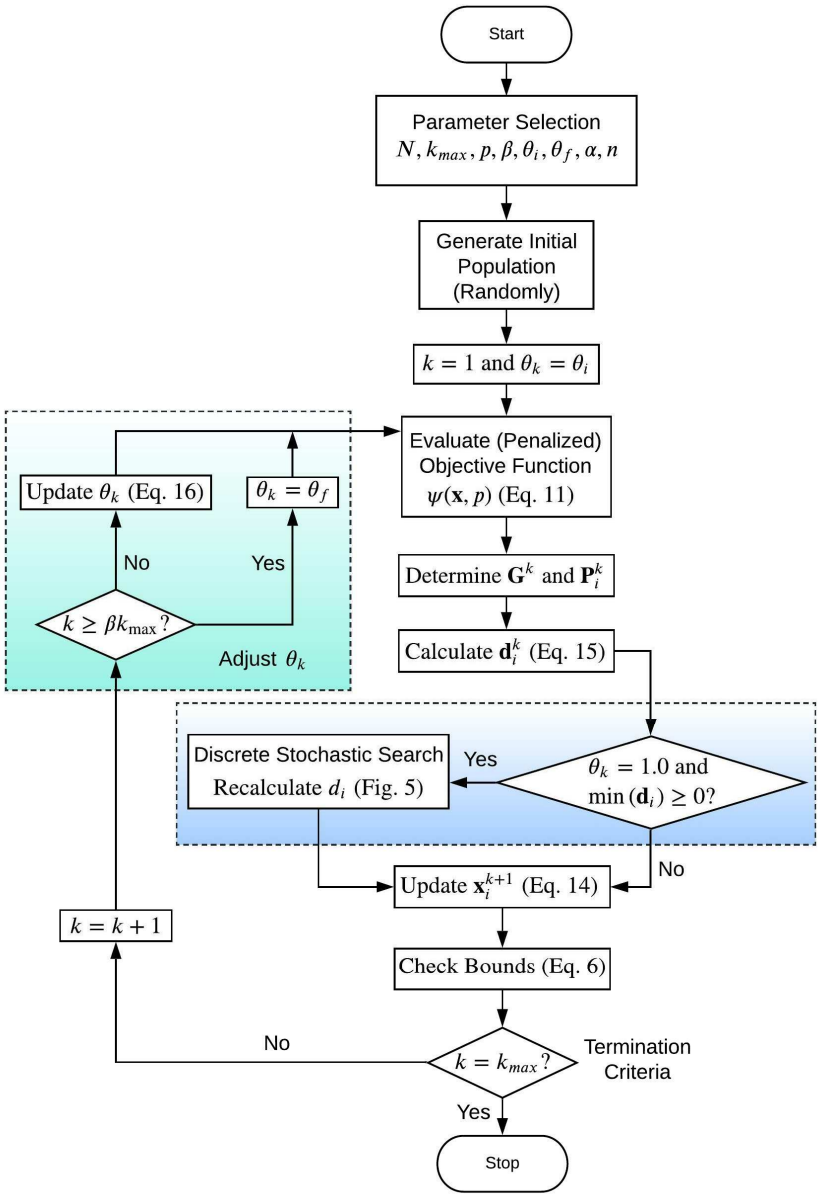

Figure 4. Flowchart of ETE optimization algorithm for discrete member sizing optimization of steel frames.

Metaheuristic design optimization of large-scale steel frames typically demands many iterations (Kaveh, 2021) to arrive at near-optimal solutions. From Eq. (15), it is clear that $\mathbf{d}_i$ approaches 0 as k becomes large. If $\mathbf{d}_i = 0$ and $\theta_k = 1.0$, the new particle $\mathbf{x}_i^{k+1}$ will remain in the same position as the global best $\mathbf{G}^k$, according to Eq. (14). Additionally, if every entry in $\mathbf{d}_i$ is equal to or greater than 0, $\mathbf{x}_i^{k+1}$ is certain to produce a worst solution than $\mathbf{G}^k$. To address this, a discrete stochastic exploitation scheme (Figure 5)

introduced in Fernández-Cabán and Masters (2018) is integrated into the ETE algorithm during late stages of the optimization process.

function $\mathbf{d}_{i,new} = \text{recalcd}(\theta_k, \mathbf{d}_i)$
  if $\theta_k = 1.0$ and $\min(\mathbf{d}_i) \geq 0$
    $\mathbf{d}_{i,new} = \text{zeros}(1, nd)$
    $j = \text{randi} \rightarrow [1 \;\; nd]$
    $a = \text{round}\left(\sqrt[3]{N_{\text{sec},j}}\right)$
    $d_{i,new,j} = \text{randi} \rightarrow [-a \;\; -1]$
    if $j = nd$
      $b = \text{round}\left(\sqrt[3]{N_{\text{sec},j-1}}\right)$
      $d_{i,new,j-1} = \text{randi} \rightarrow [0 \;\; b]$
    else
      $c = \text{round}\left(\sqrt[3]{N_{\text{sec},j+1}}\right)$
      $d_{i,new,j+1} = \text{randi} \rightarrow [0 \;\; c]$
    end
  else
    $\mathbf{d}_{i,new} \rightarrow$ Eq. (15)
  end
end

Figure 5. Discrete stochastic exploitation scheme for recalculating $\mathbf{d}_i$.

5 Case Study

A 20-story braced steel space (3D) frame structure studied by Hasançebi et al. (2011) was selected to investigate the effect of member grouping and limiting the set of available profile lists on the optimal solution. Isometric and plan views of the steel frame are shown in Figure 6. The frame comprises 416 joints and 1040 structural members. The lateral force resisting system consists of K-type bracing located

at the mid-bay in each side of the building envelope. The plan building dimensions are 45 ft (13.7 m) × 60 ft (18.3 m) and all floors are 12 ft (3.66 m) tall. Strength requirements were imposed on all structural members according to AISC-LRFD specifications [Eq. (7)]. Additionally, horizontal joint displacements in the x and y directions were limited to 1/500 of the building height (H/500) while mean inter-story drift limit for each floor was set to 1/400 of the story height (h) for all floors [i.e., δ_{allw} = h/400 in Eq. (8)]. Finally, geometric constraints [Eqs. (9) – (10)] were enforced between beam and column members framing into each other at all joints. A modulus of elasticity of E = 29,000 ksi (200 GPa) and yield stress of F_y = 50 ksi (344.7 MPa) were assumed for all structural steel members. For compressive strength calculations, the effective length factor for all beam, column, and bracing members was taken as unity.

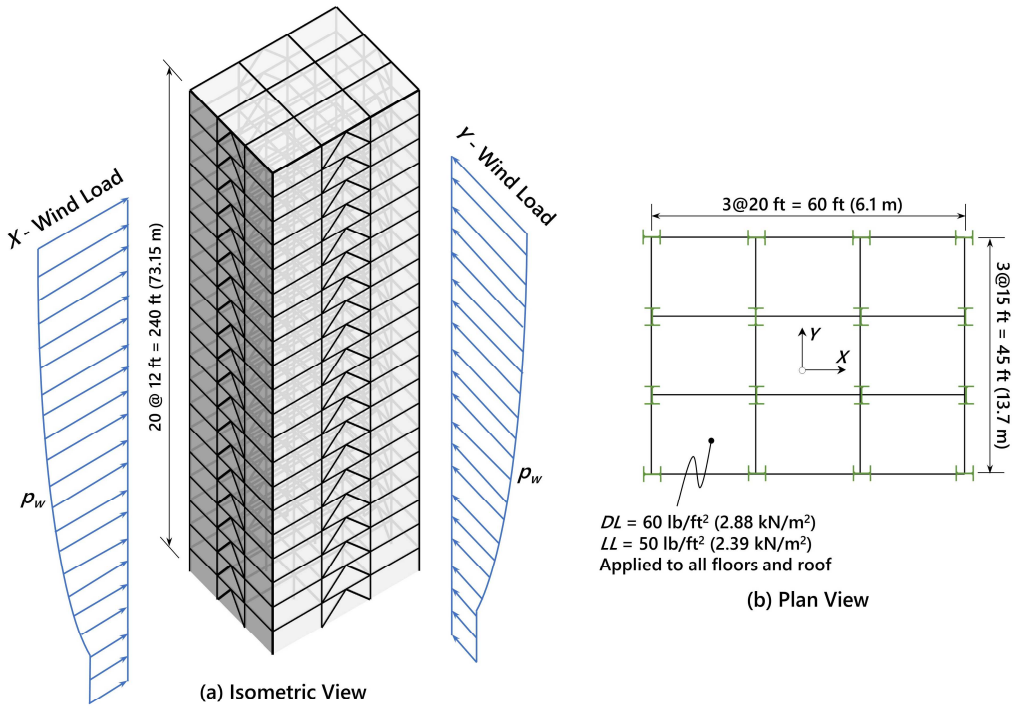

Figure 6. Isometric view (a), plan view (b), and loading condition of 3D 20-story steel frame.

5.1 Design loads

The 20-story steel frame was subjected to both gravity loads and lateral wind loads acting along the two principal building axes (i.e., x and y), as shown in Figure 6. The gravity loads consisted of uniform area dead (D) and live (L) loads of 60 lb/ft^2 (2.88 kPa) and 50 lb/ft^2 (2.39 kPa) respectively. The gravity loads were applied on the entire floor area of all 20 stories. The following basic load combinations from ASCE 7-16 (2016) were considered for LRFD strength design checks of the structural steel members:

$$1.4D \tag{17}$$

$$1.2D + 1.6L \tag{18}$$

$$1.2D + (L \; or \; 0.5W_x) \tag{19}$$

$$1.2D + \left(L \; or \; 0.5W_y\right) \tag{20}$$

$$1.2D + 1.0W_x + L \tag{21}$$

$$1.2D + 1.0W_y + L \tag{22}$$

$$0.9D + 1.0W_x \tag{23}$$

$$0.9D + 1.0W_y \tag{24}$$

In Eqs. (19) – (24), W_x and W_x are factored wind loads in the x and y direction, respectively. Design wind pressures were estimated according to ASCE 7-16 from:

$$q_z = 0.00256K_zK_{zt}K_dK_eV^2 \tag{25}$$

where q_z (lb/ft^2) is the velocity pressure at height z (ft), K_z is the exposure coefficient, K_{zt} is the topographic factor, K_d is the wind directionality factor, K_e is the ground elevation factor, and V is the basic wind speed (in mph) corresponding to a 3-sec gust at 33 ft (10-m) above ground in Exposure C (i.e., open terrain). In this study, K_z was computed based on Exposure B, K_{zt} = 1.0, K_d = 0.85, K_e = 1.0, and V = 105 mph (46.94 m/s). The design wind pressure p_w for the windward and leeward building faces were obtained from:

$$p_w = q_zG_FC_p \tag{26}$$

where G_F = 0.85 (i.e., gust factor), and C_p is the external pressure coefficient which was set to 0.8 and –0.5 for the windward and leeward faces respectively.

ASCE 7-16 (2016) LRFD load combinations require multiple structural analyses to independently apply the design loads (wind-x, wind-y, dead, and live) on the steel frame. In the present work, three structural analyses were performed to assess the fitness of each candidate design (i.e., particle) under dead and wind loads along the two orthogonal directions (i.e., x and y). Live loads were determined from dead load analysis since both forces were applied on the structure in the same manner and only the magnitude was scaled accordingly.

5.2 Parallel processing and optimization parameters

Linear elastic structural analysis and the ETE optimization algorithm were coded and executed in MATLAB. Due to the relatively large size of the frame and the vast domain of candidate designs (i.e., search space), a portion of the optimization runs performed on the frame were offloaded to the ACRES high-performance computing (HPC) cluster at Clarkson University. The ACRES cluster consists of 62 compute-nodes, 2440 CPU cores, 8TB of total memory, and four (4) GPUs—for a total computing power of more than 160 teraflops. Structural analysis and optimization scripts were sent to multiple workers (i.e., nodes) on the ACRES cluster as batch jobs and parallel processing—using the *parfor* command in MATLAB—was implemented to simultaneously evaluate candidate designs and reduce computational time. The bulk of the optimization runs were performed using 6–8 ACRES workers (i.e., nodes). Additional optimization runs were performed from a personal computer—Intel(R) Core(TM) i7-10700K CPU @ 3.80 GHz with 64 GB RAM—and parallel processing was also applied using all available cores on the local machine.

In all problems, optimization parameters were set to N = 100, p = 0.1, $\theta_i = 0.5$, $\theta_f = 1.0$, $\alpha = 0.6$, β = 0.25, and n = 3. Parameters θ_i, θ_f, and β are specific to ETE and their values control the exploration and exploitation of the algorithm at different stages of the optimization process. The parameter θ_i was chosen so that equal influence from $\mathbf{G}^k$ and $\mathbf{P}_i^k$ was given to initial candidate designs, while θ_f was set to unity to limit the search around the global best during late stages of the optimization process. The population size of N and α were chosen based on values selected from other population-based algorithms found in recent research studies of large-scale steel frames (e.g., Azad and Hasançebi, 2015;

Azad, 2021; Kaveh, 2021). Finally, the β parameter in Eq. (16) selected to promote exploration of the design space during the first fourth (k_{max}/4) of the optimization process and was calibrated during preliminary optimization runs based on N and k_{max}. Fernández-Cabán and Masters (2018) demonstrated that the final (optimal) solution was relatively insensitive to the value of β in the case of three multi-story steel frames, although a faster improvement in the objective function (i.e., frame weight) was observed when selecting lower β values (i.e., limiting the exploration stage and prolonging the exploitation stage).

5.3 Member grouping

The effect of member grouping was investigated by modifying the total number of member groups (MG) used to optimize the 20-story steel frame. Specifically, four MG cases consisting of 60, 70, 90, and 100 total member groups (i.e., design variables) were examined and are illustrated in Figure 7. Structural symmetry about the principal x and y axes of the building were imposed on the four MG cases. Members on consecutive stories were collected into groups according to their type and spatial location on the structure, as shown in Table 1. The total number of member groups for a specific MG case can be calculated as the sum of the member groups per floor multiplied by half the number of floors of the building. For instance, the total number of groups for MG060 is 6 × 20 stories/2 = 60 groups.

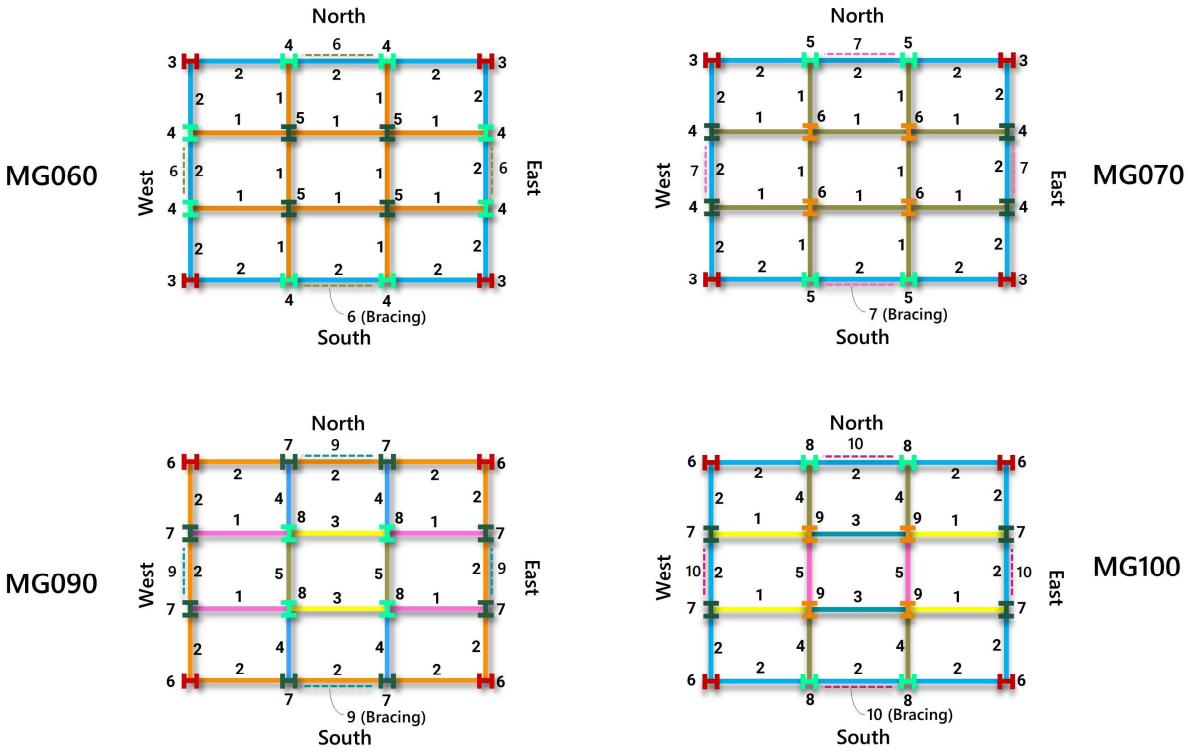

Figure 7. Member group cases considered for the 20-story steel frame.

Member group MG060 corresponds to the grouping arrangement adopted in Hasançebi et al. (2011), where all interior beams share the same member group and perimeter beams form a separate member group. The inner columns, corner columns, and remaining exterior columns make up three unique member groups, respectively, resulting in 30 total column groups throughout the building (i.e., 3 × 20 stories/2 = 30). Similar arrangements to MG060 are commonplace in literature (e.g., Hasançebi et al., 2011; Kaveh and Bolandgerami, 2017; Kaveh, 2021) for the optimal design of large-scale steel frames. Member group MG070 resembles MG060 except that exterior column groups (North-South and East-West) now constitute two distinct member groups in MG070. MG060 and MG090 share the same number of column groups but MG090 has five beam member groups per story. Specifically, the perimeter beams are all part of one member group (this is the case for all MG arrangements), and the inner beams are divided into four member groups with parallel beams being grouped together (Figure 7). Finally, group MG100 has four unique column groups per story where inner columns, corner columns, and exterior

column groups (North-South and East-West) are part of a separate member group, resulting in 40 total column groups for MG100. In all four cases, K-bracing members are collected into a single member group. Thus, in each case, there are 10 total bracing groups.

Table 1. Structural member grouping (i.e., design variable) cases considered for the 20-story frame.

Structural Members	Member Group ID			
	MG060	MG070	MG090	MG100
Inner Beams (East-West)	1	1	1	1
Inner (Core) Beams (East-West)	1	1	3	3
Inner Beams (North-South)	1	1	4	4
Inner (Core) Beams (North-South)	1	1	5	5
Perimeter Beams	2	2	2	2
Corner Columns	3	3	6	6
Exterior Columns (East-West)	4	4	7	7
Exterior Columns (North-South)	4	5	7	8
Inner Columns	5	6	8	9
K-Bracing Members	6	7	9	10
Total Member Groups (Design Variables)	60	70	90	100

5.4 Discrete set of steel profiles

A profile list (PL) constitutes a discrete set of available structural steel shapes that can be used as framing members. Table 2 reports the four PL cases considered in this study. The first profile list (PL1) is the largest pool size of available structural shapes, with 263 standard W-Shape steel sections ranging in size from W8–W44 for column, beam, and bracing member groups. This profile list (PL1) combined with member group MG100 results in the largest design space of all MG/PL combinations considered. The second profile list (PL2) includes a subset of 117 steel shapes ranging in size from W10–W18 for column members and 133 steel shapes ranging from W21–W44 for beam and bracing members. This case allows for a relatively thorough search of possible steel shapes but remains limited enough to be conservative with respect to computational time. Profile list PL3 further reduces the profile and only contains 70 W-shapes ranging from W14–W18 for the columns and 72 steel shapes ranging in size from W21–W30 for the beams and bracing members. Finally, profile list PL4 is the smallest profile list consisting of 36 W14 steel shapes that can be assigned to column members and 21 W24 steel shapes to

size the beams bracing members. Profile list PL4 was chosen in this study given the prevalence in previous studies (Chan and Grierson, 1993; Chan and Chui, 2006; Walls and Elvin, 2010b; Spence and Kareem, 2014).

Table 2. Profile list cases considered for the 20-story frame.

W-Shape Profile List	W-Shapes Steel Shapes		
	Columns	Beams	K-Bracing
PL1	W8×10–W44×335 (263)	W8×10–W44×335 (263)	W8×10–W44×335 (263)
PL2	W10×12–W18×311 (117)	W21×44–W44×335 (133)	W21×44–W44×335 (133)
PL3	W14×22–W18×311 (70)	W21×44–W30×391 (72)	W21×44–W30×391 (72)
PL4	W14×22–W14×730 (36)	W24×55–W24×370 (21)	W24×55–W24×370 (21)

6 Results and Discussion

A total of 105 independent ETE optimization runs were performed on the 20-story steel frame. First, 16 experimental cases representing all possible combinations between the four member groups (MG) and four profile list (PL) cases were considered. Due to the stochastic nature of the ETE algorithm, each case was repeated five times to obtain a statistical measure of the variability observed in the final design (i.e., weight). This generated an initial testing matrix of 4 member groups (MG) × 4 profile lists (PL) × 5 runs/case = 80 independent runs. The maximum number of iterations was chosen as the termination criteria and set to k_{max} = 500 for the first 80 test runs. An additional series of optimization experiments were conducted to further investigate convergence of the ETE algorithm, particularly for the MG case with the largest number of design variables (i.e., MG100).

6.1 Initial optimization runs

Figure 8 includes the iteration history of the penalized weight ($\psi(\mathbf{x})$) for all 16 combinations of member grouping and W-shape profile list cases. Each curve represents the mean value of $\psi(\mathbf{x})$ obtained from five independent ETE optimization runs. The four subplots in Figure 8 all reveal a steeper drop in $\psi(\mathbf{x})$ for MG060 and MG070 at early iterations (k < 80), while member groups with greater number of design variables (i.e., MG060 and MG070) consistently show a much shallower descent and slower improvement

of $\psi(\mathbf{x})$. Further, it is evident from Figure 8a (PL1) that the final penalized weight at k_{max} = 500 shows high variability in the results and the final solution seems to be strongly dependent on the number of member groups. For PL1, MG090 and MG100 settled on final weights of approximately 825 kips (3.67 MN), while MG060 was able to achieve a final mean weight of 658.6 kips (2.93 MN). It is expected for cases with a larger number of member groups (e.g., MG100) to produce lighter designs since they are less constrained on the different number steel shapes that can be selected. This indicates that k_{max} may need to be increased for cases with a larger number of member groups (i.e., MG090 and MG100) to provide ETE algorithm sufficient time to find solutions that are closer to the global optimum. Conversely, Figure 8d (PL4) shows how all member group cases rapidly converge to very similar solutions at k ~ 200. Figures 8b and 6c illustrate the two PL cases with design spaces that lie between the PL1 and PL4 cases. Comparable results are observed in Figure 8b for the four MGs with only slight differences in the final penalized weight. Like PL1, MG060 generated the best final weight for PL2. Finally, the subplot corresponding to PL3 shows more tightly packed $\psi(\mathbf{x})$ curves for the four MG cases when compared to PL2. Additionally, the four $\psi(\mathbf{x})$ curves in Figure 8c appear to converge on an optimal design at k > 400.

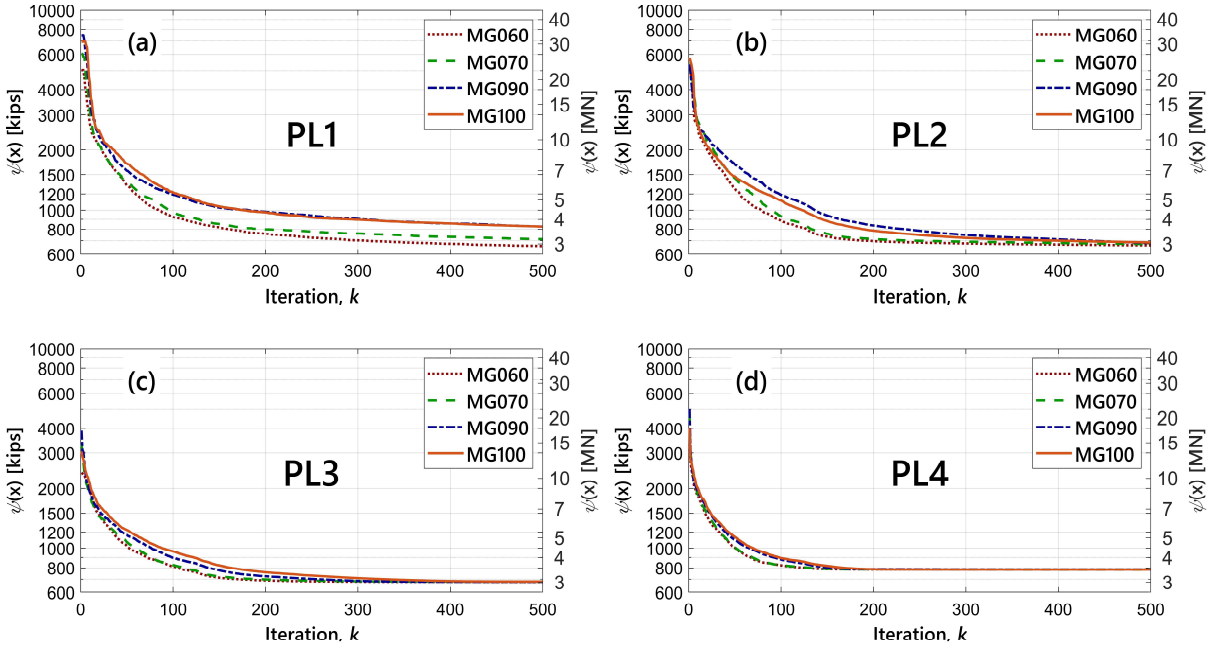

Figure 8. ETE iteration histories of mean penalized weight $\psi(\mathbf{x})$ for W-shape profile lists (a) PL1, (b) PL2, (c) PL3, and (d) PL4.

Table 3 summarizes the statistics from five independent ETE runs of $\psi(\mathbf{x})$ obtained in each of the 16 cases executed. It is evident that the variability of the final weight is noticeably smaller when the set of available steel shapes is reduced to a subset of discrete sections for k_{max} = 500. For instance, the coefficient of variation (CoV) for PL1 ranged between 2.098–7.923% while PL4 cases were CoV = 0.084–0.235%. A representative ETE iteration history for the independent runs corresponding to PL4/MG100 is depicted in Figure 9. Yet, the lowest penalized weight from all 80 runs was achieved by PL1/MG060 ($\psi(\mathbf{x})$ = 624.9 kips (2.78 MN)). At the same time, the worst run (i.e., heaviest design) was produced by PL1/MG100 ($\psi(\mathbf{x})$ = 938.4 kips (4.17 MN)), which represents the case with the largest design space. The ETE iteration for this worst run is illustrated in Figure 10. For most optimization runs, strength, drift, and geometric constraints were satisfied when the final design was reached (at k_{max}) and only negligeable violations ($C(\mathbf{x})$ < 0.02) were observed in some cases. The number of structural analyses for each optimization run was 3 analyses (see Section 5.1) × 100 particles × 500 iterations = 150,000.

Table 3. Final penalized weights found by the ETE algorithm for the 20-story frame (k_{max} = 500).

Run ID	Profile List	Member Group	Final Penalized Weight, $\psi(\mathbf{x})$, kips (MN)						Standard Deviation, kips (MN)		CoV (%)
			Maximum (worst run)		Mean		Minimum (best run)				
T001–T005	PL1	MG060	677.7	(3.015)	658.6	(2.930)	624.9	(2.780)	19.1	(0.085)	2.908
T006–T010		MG070	749.7	(3.335)	712.5	(3.169)	680.8	(3.028)	21.9	(0.098)	3.080
T011–T015		MG090	851.3	(3.787)	825.6	(3.672)	807.6	(3.592)	17.3	(0.077)	2.098
T016–T020		MG100	938.4	(4.174)	824.8	(3.669)	734.6	(3.268)	65.4	(0.291)	7.923
T021–T025	PL2	MG060	668.6	(2.974)	664.3	(2.955)	661.6	(2.943)	2.43	(0.011)	0.365
T026–T030		MG070	679.0	(3.020)	673.5	(2.996)	668.2	(2.973)	3.97	(0.018)	0.590
T031–T035		MG090	693.6	(3.085)	680.8	(3.028)	661.9	(2.944)	10.9	(0.049)	1.603
T036–T040		MG100	699.8	(3.113)	686.5	(3.054)	674.2	(2.999)	10.3	(0.046)	1.497
T041–T045	PL3	MG060	683.2	(3.039)	677.1	(3.012)	672.5	(2.992)	3.68	(0.016)	0.544
T046–T050		MG070	681.0	(3.029)	679.3	(3.022)	676.2	(3.008)	2.01	(0.009)	0.295
T051–T055		MG090	682.3	(3.035)	678.0	(3.016)	674.2	(2.999)	3.46	(0.015)	0.511

T056–T060		MG100	693.3	(3.084)	680.6	(3.027)	674.3	(2.999)	6.61	(0.029)	0.972
T061–T065	PL4	MG060	785.6	(3.494)	784.5	(3.490)	783.5	(3.485)	0.66	(0.003)	0.084
T066–T070		MG070	786.2	(3.497)	783.4	(3.485)	780.5	(3.472)	1.83	(0.008)	0.233
T071–T075		MG090	786.7	(3.500)	785.5	(3.494)	784.7	(3.490)	0.94	(0.004)	0.120
T076–T080		MG100	788.1	(3.506)	784.5	(3.490)	782.8	(3.482)	1.84	(0.008)	0.235

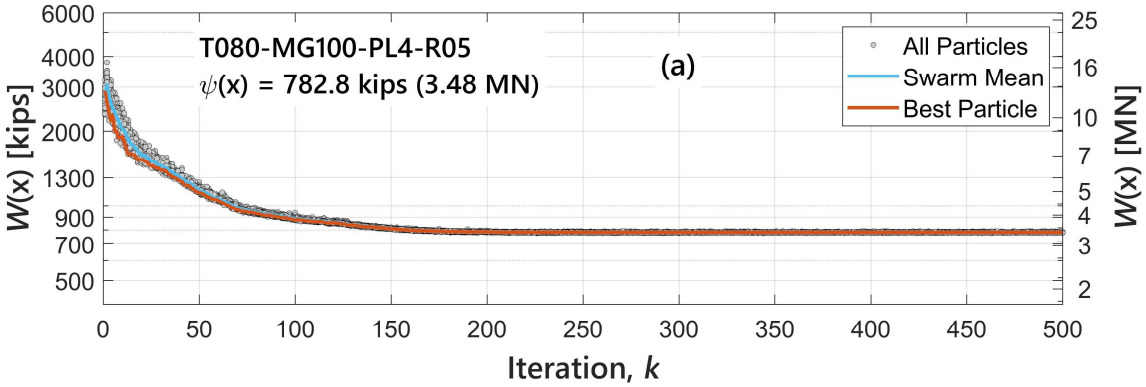

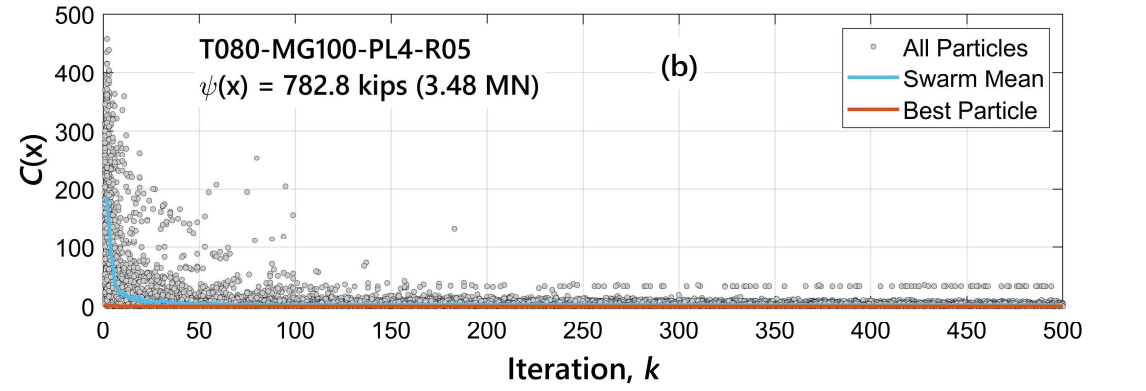

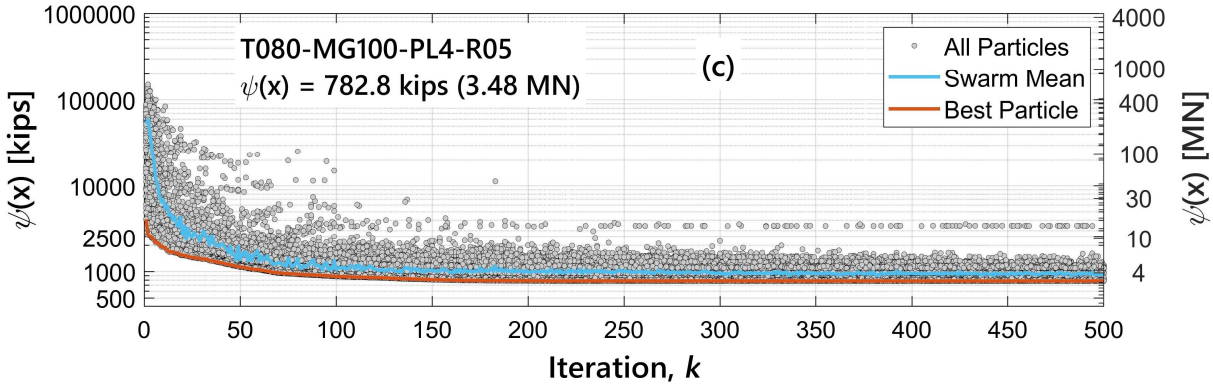

Figure 9. ETE iteration histories of (a) unpenalized weight, (b) penalty function, and (c) penalized weight corresponding to optimization run T080-MG100-PL4-R04.

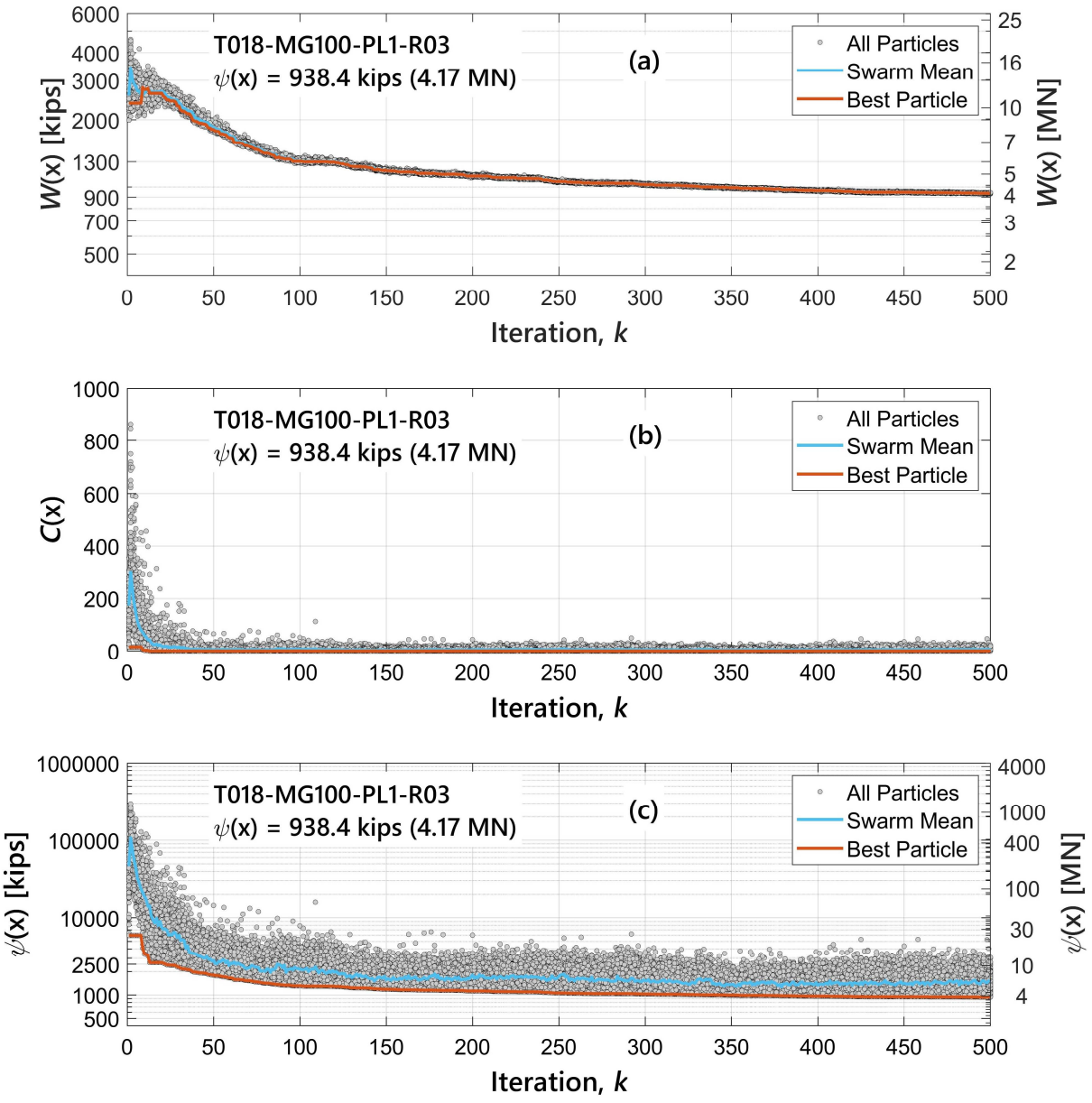

Figure 10. ETE iteration histories of (a) unpenalized weight, (b) penalty function, and (c) penalized weight corresponding to optimization run T018-MG100-PL1-R03.

The set of optimal solutions found from the initial series of optimization runs were generally lighter that the optimal design reported in Hasançebi et al. (2011) for the same 20-story frame. Yet, comparison

between the two studies is problematic due to differences in design procedures and profile list of steel shapes included in the optimization. For instance, Hasançebi et al. (2011) used ASD-AISC (1989) specifications and load combinations, and a lower yield strength was assumed for strength checks compared to the present work (F_y = 36 ksi vs. F_y = 50 ksi). Further, the designation bounds for the pool of W-shapes assigned to beams and bracing members was not reported. Lastly, the present work chose a lower overall lateral deflection limit than the Hasancebi et al. (2011) study. However, it was concluded that the difference in overall drift limits (H/400 vs. H/500) was deemed irrelevant since the optimal designs were controlled by inter-story drift, stress ratios, and/or geometric constraints. However, this may not be the case for more slender systems where the overall drift constraint may govern.

6.2 Dependence of k_{max} on optimal design

Statistical results obtained from the initial series of optimization runs indicate that when the number of member groups (i.e., design variables) was reduced, the ETE algorithm consistently converged to near-optimal solutions with minimal fluctuations in the final design over multiple runs. However, significantly larger design domains (e.g., PL1/MG100 combination) revealed greater variability in the final solutions, thus suggesting that convergence of the ETE algorithm for these runs required a greater number of iterations (k_{max}). This section examines the effect of k_{max} on the quality of the final solution for solution spaces of considerably larger sizes. Table 4 lists the k_{max} used to execute the second series of ETE runs conducted on the 20-steel frame.

Table 4. Testing matrix for second series of ETE optimization runs performed on the 20-story frame.

Run ID	W-Shape Profile List	Member Grouping	k_{max}	No. of Independent Runs
T081–T085	PL1	MG100	2000	5
T086–T090	PL1	MG100	4000	5
T091–T095	PL2	MG100	3000	5
T096–T100	PL3	MG100	2000	5
T101–T105	PL4	MG100	1000	5

Figure 11 depicts the final weight $\psi(\mathbf{x})$ as a function of k_{max} for all ETE optimization runs corresponding to profile list PL1 and MG100 grouping configuration. This PL/MG combination represents

the largest design space from all cases considered in this study. A dramatic reduction in both the variability and quality of $\psi(\mathbf{x})$ can be observed in Figure 11 when k_{max} is increased. For instance, the best run of $\psi(\mathbf{x})$ was reduced by 33.6%—734.6 kips (3.27 MN) vs. 487.9 kips (2.17 MN)—when k_{max} was increased from 500 to 4000. Further, the CoV dropped from 7.923 % (k_{max} = 500) to 1.019 % (k_{max} = 4000), as shown in Tables 3 and 5, respectively. However, this came at the expense of increased computational time from 4.4 hr (k_{max} = 500) to 29.7 hr (k_{max} = 4000). Each of the five optimization runs with k_{max} = 4000 (T086–T090) required 1.2×10^6 structural analyses (i.e., 3 analyses × 100 particles × 4000 iterations = 1.2×10^6). When comparing weight statistics for PL2/MG100 executed over k_{max} = 500 (Table 3) and k_{max} = 3000 (Table 5), only a 3.22% reduction in the mean final weight $\psi(\mathbf{x})$ was observed. Results reported in Table 5 for PL3 and PL4 indicate that negligible improvements in weight statistics occur when k_{max} is increased.

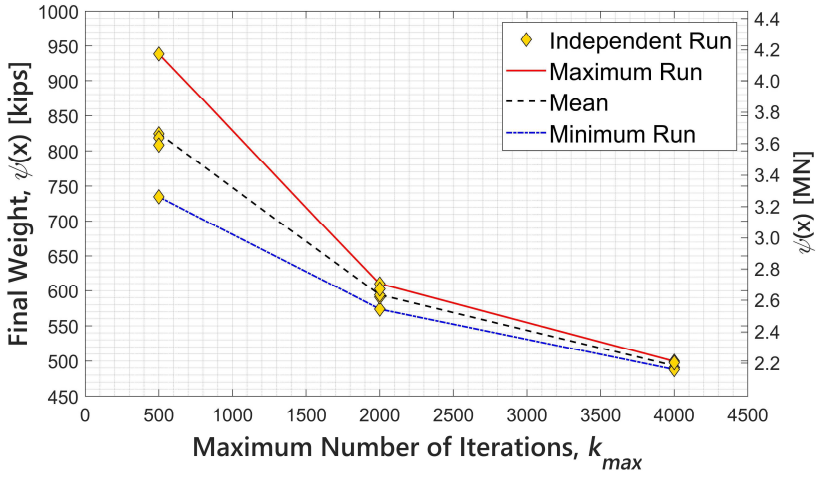

Figure 11. Final weights found by ETE algorithm for over multiple k_{max} values (PL1 and MG100).

Table 5. Statistics of final penalized weight for the second series of ETE optimization runs performed on the 20-story frame.

W-Shape Profile List	k_{max}	Final Penalized Weight, $\psi(\mathbf{x})$, kips (MN)			Standard Deviation (kips)	Coefficient of Variation (%)
		Maximum (worst run)	Mean	Minimum (best run)		

PL1	4000	499.5 (2.222)	493.2 (2.194)	487.9 (2.170)	5.025 (0.0223)	1.019
PL2	3000	669.0 (2.976)	664.4 (2.955)	658.0 (2.927)	4.858 (0.0216)	0.731
PL3	2000	688.9 (3.064)	682.0 (3.034)	672.8 (2.993)	6.516 (0.0290)	0.955
PL4	1000	784.6 (3.490)	782.7 (3.481)	780.6 (3.472)	1.447 (0.0064)	0.185

Mean $\psi(\mathbf{x})$ iteration histories of runs T081–T105 are plotted in Figure 12. Weight optimization curves for all four PLs appear to converge to near-optimal solutions. In the case of PL1 and MG100, the mean $\psi(\mathbf{x})$ shows a steady (nearly linear) improvement from iteration 1000 up to k ~ 3200 before plateauing toward the final solution—$\psi(\mathbf{x})$ = 493.2 kips (2.19 MN). The persistent improvement in $\psi(\mathbf{x})$ is primarily boosted by the discrete stochastic routine integrated into the ETE algorithm during late stages of the optimization process (Fernández-Cabán and Masters, 2018). The best run (i.e., lightest design) from PL1/MG100 (T089-MG100-PL1-R04) is illustrated in Figure 13.

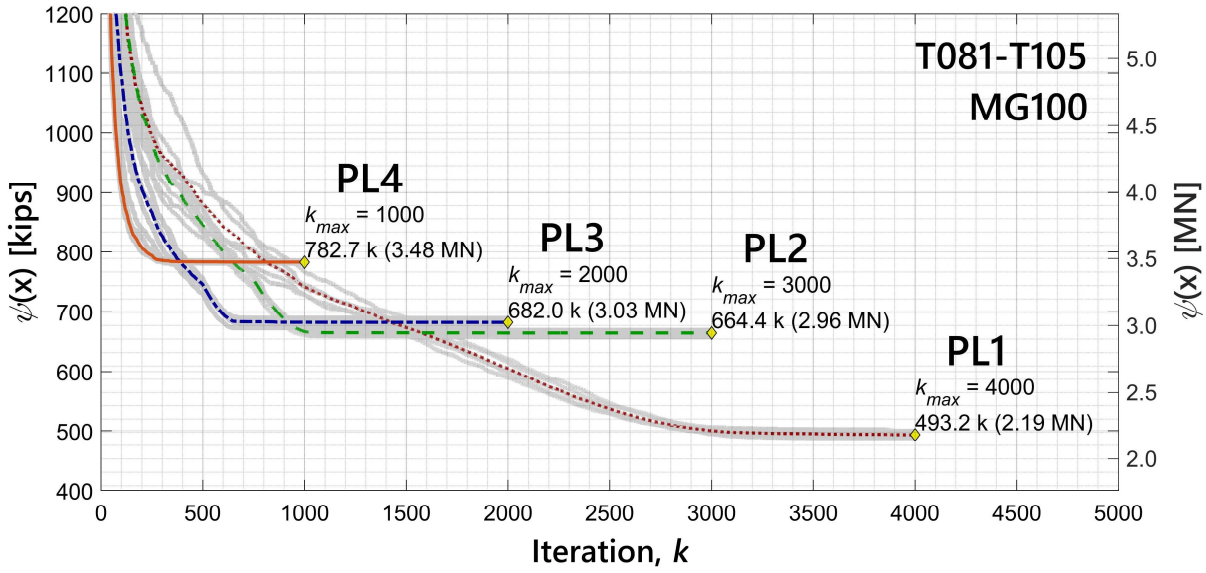

Figure 12. ETE iteration histories of mean penalized weight for the four PL cases (MG100).

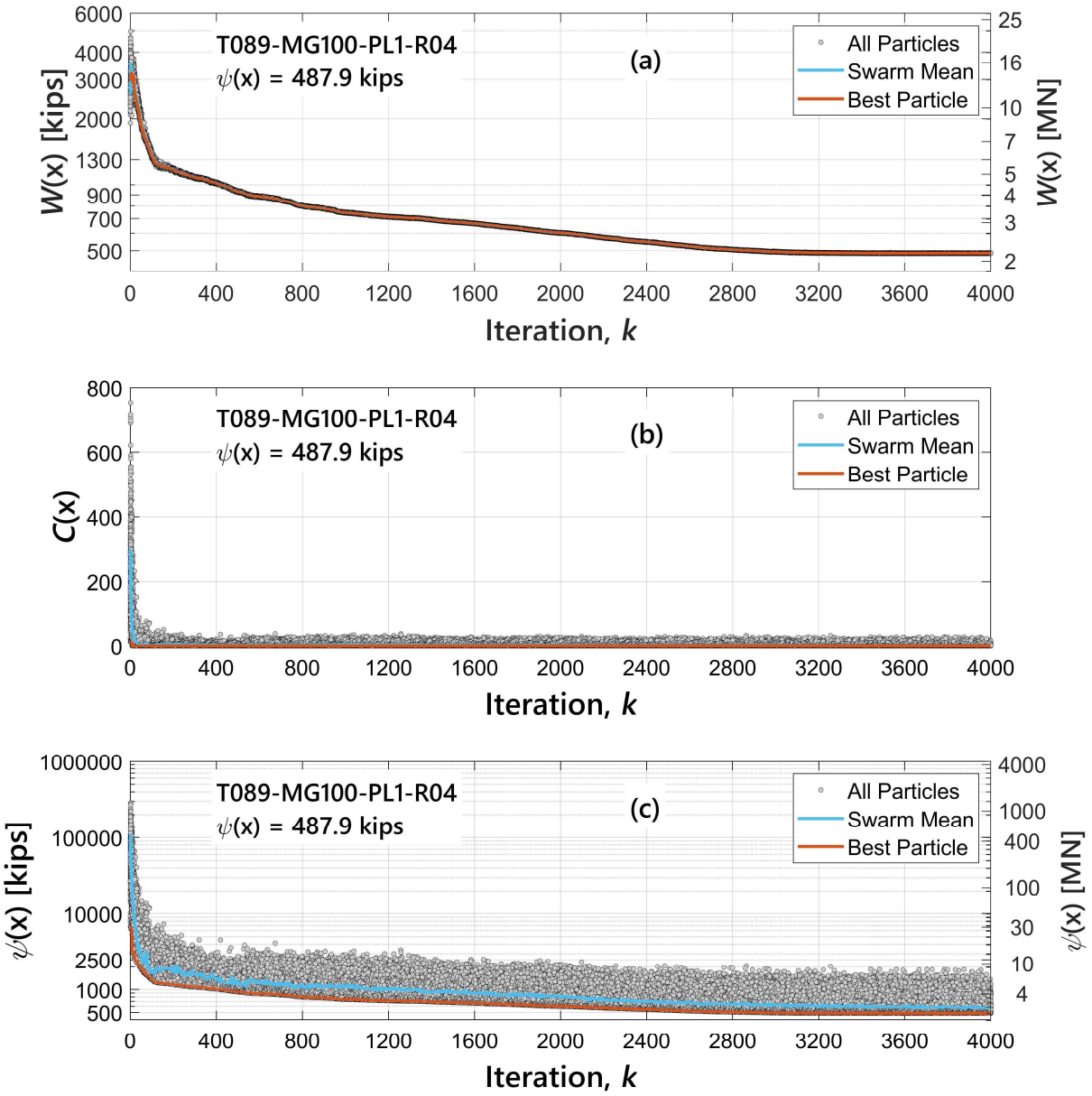

Figure 13. ETE iteration histories of (a) unpenalized weight, (b) penalty function, and (c) penalized weight for optimization run T089-MG100-PL1-R04.

Figures 14 and 15 display the final member sizes, inter-story drift, and load-capacity ratios ($LCRs$) for independent runs T089-MG100-PL1-R04 (k_{max} = 4000) and T105-MG100-PL4-R05 (k_{max} = 1000). The linewidth of the structural members is proportional to the depth of the final W-Shapes found by the ETE algorithm. Run T089-MG100-PL1-R04 (Figure 14) shows how, for some stories, the inter-story drift

along the x direction reached the drift limit (h/400) and a significant number of LCR values for column, beam, and bracing members approached (or reached) the capacity limit (LCR = 1.0). In contrast, inter-story drift values for test T105-MG100-PL4-R05 (Figure 15) are comfortably short of the inter-story drift limit and only column members show $LCRs$ ~ 1.0, while beam and bracing members are well below the LCR limit. Yet, the relative member sizes illustrated in Figure 14 suggests a rather arbitrary arrangement of steel shapes which may greatly complicate the construction of the frame. This is not the case for T105-MG100-PL4-R05 (Figure 15), where a more uniform distribution of member sizes is enforced as a direct result of limiting the selection of available steel shapes (see Table 2). However, this comes at the expense of increased weight and impairs the ETE algorithm from approaching target serviceability (i.e., inter-story drift) and strength (i.e., LCR) limit states.

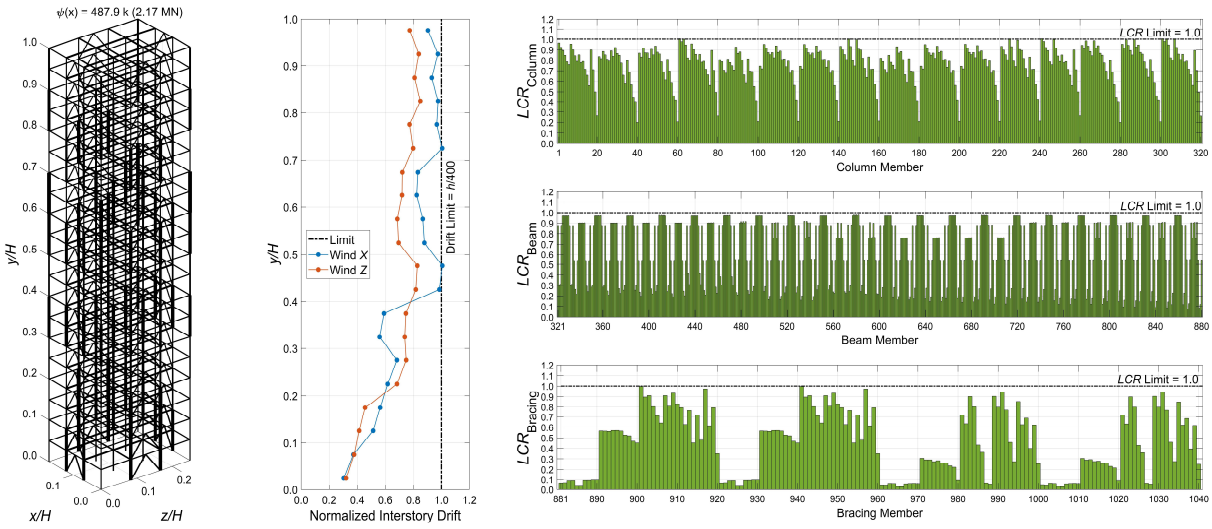

Figure 14. Relative member sizes, inter-story drift, and load-capacity ratios (LCR) obtained from independent run T089-MG100-PL1-R04 (k_{max} = 4000).

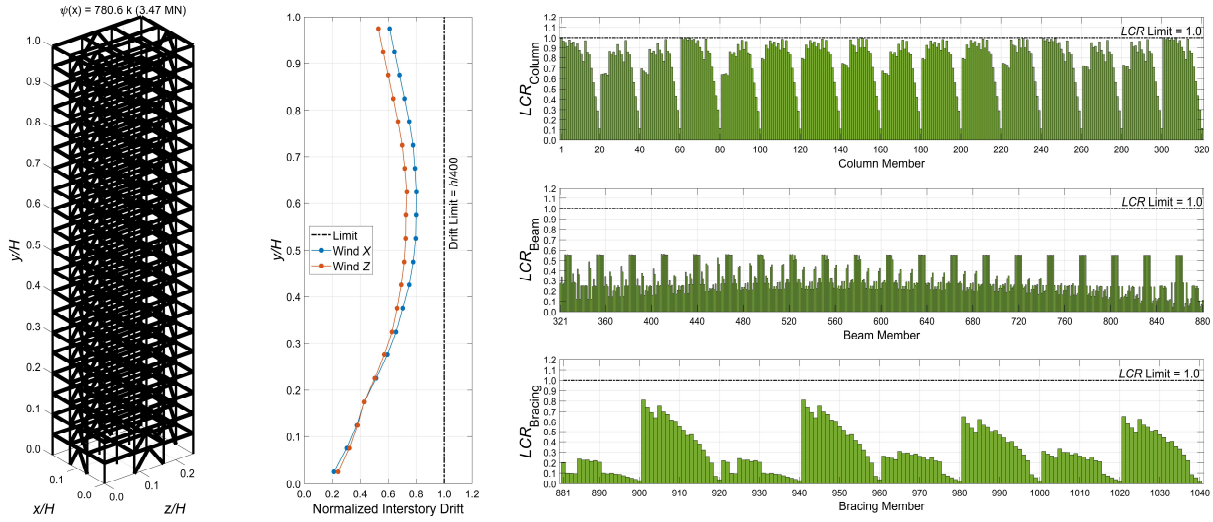

Figure 15. Relative member sizes, inter-story drift, and load-capacity ratios (LCR) obtained from independent run T105-MG100-PL4-R05 (k_{max} = 1000).

Extruded 3D visuals of the final member sizes for the first story of the 20-story frame are presented in Figure 16 for runs T089-MG100-PL1-R04 and T105-MG100-PL4-R05. The extruded geometry of the structural members is shown to scale. Overall, PL1 found significantly lighter sections than PL4 for many of the structural members except the inner column groups and the exterior columns on the East-West ends of the building. For example, exterior beams for the PL1 case (Figure 16a) were sized down to W8 × 24 compared to W24 × 55 for PL4 (Figure 16b). Similar behavior was observed for beam members located in subsequent stories, causing faster weight accumulation for PL4 in relation to PL1. In both PL1 and PL4, the heaviest members came from exterior columns connected to the bracing members, while inner and corner column groups achieved much lighter steel sections. Finally, bracing and beam members for PL4 appeared to reach the lower bound of available W24 shapes (i.e., W24 × 55). Optimal steel sections obtained for the PL2 and PL3 cases are reported in Table 6.

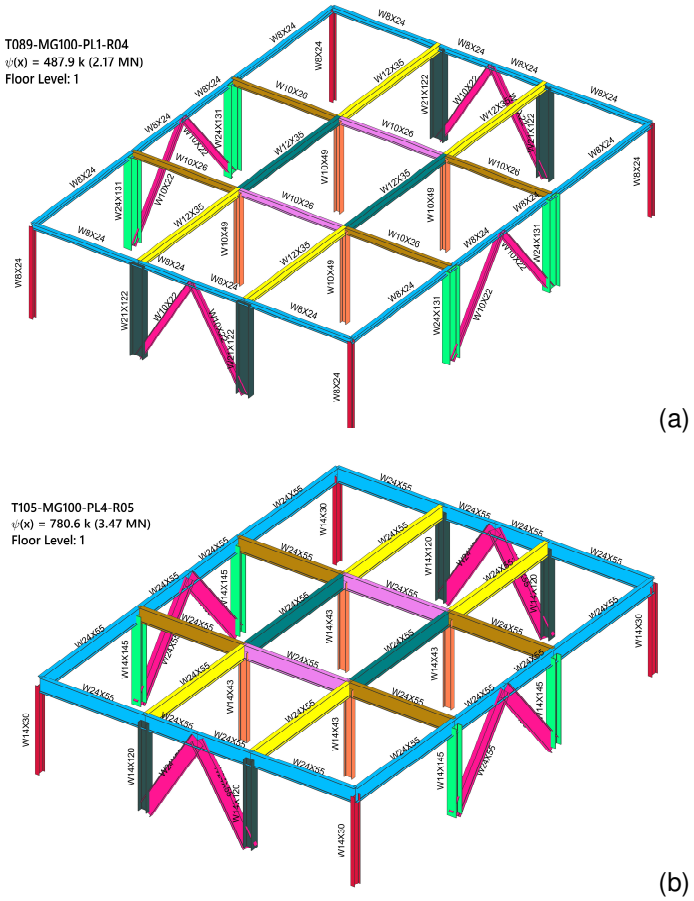

Figure 16. Optimal W-shapes for the first story of the 20-story frame from runs (a) T089-MG100-PL1-R04 and (b) T105-MG100-PL4-R05.

Table 6. Optimal W-shapes found from best ETE runs for the first story of the 20-story frame (MG100).

Member Group ID (MG100)	Structural Members	Final Steel (W-shape) Profiles			
		PL1	PL2	PL3	PL4
1	Inner Beams (East-West)	W12 × 35	W21 × 44	W21 × 44	W24 × 55
2	Perimeter Beams	W8 × 24	W21 × 44	W21 × 44	W24 × 55
3	Inner (Core) Beams (East-West)	W12 × 35	W21 × 44	W21 × 44	W24 × 55
4	Inner Beams (North-South)	W10 × 26	W21 × 44	W21 × 44	W24 × 55
5	Inner (Core) Beams (North-South)	W10 × 26	W21 × 44	W21 × 44	W24 × 55
6	Corner Columns	W8 × 24	W12 × 26	W14 × 34	W14 × 30
7	Exterior Columns (East-West)	W21 × 122	W14 × 132	W14 × 109	W14 × 120
8	Exterior Columns (North-South)	W24 × 131	W18 × 143	W18 × 143	W14 × 145
9	Inner Columns	W10 × 49	W14 × 34	W18 × 50	W14 × 43
10	Bracing Members	W10 × 22	W21 × 44	W21 × 44	W24 × 55

7 Conclusions

This study performed a robust investigation of member grouping and steel profile list effects on a real-world 20-story 3D steel frame. A series of independent structural optimization runs were performed on the steel frame for 16 unique member grouping and steel (W-Shape) profile list configurations to regulate the size of the discrete solution space and quantify the effect on the optimal design. The following conclusions can be drawn from this study:

- The lightest optimal design found was achieved by the PL1/MG100 combination, which constitutes the largest search space of the cases considered. Yet, larger k_{max} values were needed for the ETE algorithm to converge due to the size and complexity of the solution space. Further, the PL1/MG100 case produced the greatest number of distinct steel shapes—due to larger number of member groups and available steel profiles—which can complicate traditional construction practices.
- When comparing the best ETE optimization runs among the different profile list (PL) cases, PL4—i.e., the smallest subset of available steel profiles—consistently generated the heaviest designs. However, PL4 used the least number of unique steel shapes which can translate to lower costs associated with bulk purchasing and fabrication cost.
- Profile list PL4 was insensitive to changes to the set of member group arrangements investigated in this study.
- Reducing the number of member groups improved convergence time of the ETE algorithm for all profile list (PL) cases tested in this study.
- For optimization problems with large design spaces (PL1/MG100), the variability and quality of the optimal design (i.e., final weight) obtained by the ETE algorithm was strongly dependent on the termination criteria (k_{max}).
- The ETE algorithm seemed to perform a robust search of the largest design space considered (PL1/MG100) and minimal fluctuations in the final weight were found over multiple runs. However,

achieving convergence demanded significantly longer runtimes compared to cases with smaller solution spaces (e.g., PL4/MG60).

While the conclusions outlined in this study may apply to other steel frame structures with similar topologies and loading conditions, further studies are needed to investigate the dependence of member grouping and pool size of discrete sections on the optimal design of systems with geometries that significantly deviate from the case study considered. Additionally, future research opportunities may include the development of advanced optimization methods to accurately quantify fabrication and constructability costs and integrate non-structural (e.g., architectural) constraints into the optimization problem. Finally, multi-objective design procedures can also be explored to accurately map the tradeoff between competing objectives such as weight minimization and constructability of large-scale structural systems.

8 Acknowledgements

Some of the research work performed in this study was supported by the National Science Foundation (NSF) through the research experience for undergraduate (REU) site at Clarkson University under Grant No. 1852102. The authors would also like to thank Clarkson University and the Office of Information Technology for providing computational resources and support that contributed to these research results. Additional computational resources for this grant were provided by NSF under Grant No. 1925596 (ACRES cluster). Any opinions, findings, and conclusions or recommendations expressed in this study are those of the authors and do not necessarily reflect the views of NSF.

9 References

American Institute of Steel Construction (AISC) (2016) Manual of steel construction, load & resistance factor design (LRFD), 15th Edition, Chicago, USA.

American Institute of Steel Construction (AISC) (1989) Manual of steel construction, allowable stress design (ASD), 9th Edition, Chicago, USA.

ASCE 7-16 (2016) Minimum design loads for building and other structures. American Society of Civil Engineers, Virginia, USA

Arora, J. S. (2000). Methods for discrete variable structural optimization. In Advanced Technology in Structural Engineering (pp. 1-8).

Azad, S. K. (2021). Design optimization of real-size steel frames using monitored convergence curve. *Structural and Multidisciplinary Optimization*, *63*(1), 267-288.

Azad, S. K., & Hasançebi, O. (2015). Computationally efficient discrete sizing of steel frames via guided stochastic search heuristic. Computers & Structures, 156, 12-28.

Barbosa, H. J., Lemonge, A. C., & Borges, C. C. (2008). A genetic algorithm encoding for cardinality constraints and automatic variable linking in structural optimization. *Engineering Structures*, *30*(12), 3708-3723.

Barbosa, H. J., & Lemonge, A. C. (2005, June). A genetic algorithm encoding for a class of cardinality constraints. In *Proceedings of the 7th annual conference on Genetic and evolutionary computation* (pp. 1193-1200).

Biedermann, J. D., & Grierson, D. E. (1995). A generic model for building design. Engineering with Computers, 11(3), 173-184.

Biedermann, J. D. (1997). Representing design knowledge with neural networks. Computer-Aided Civil and Infrastructure Engineering, 12(4), 277-285.

Biedermann, J. D., & Grierson, D. E. (1996). Training and using neural networks to represent heuristic design knowledge. Advances in Engineering Software, 27(1-2), 117-128.

Boscardin, J. T., Yepes, V., & Kripka, M. (2019). Optimization of reinforced concrete building frames with automated grouping of columns. *Automation in Construction*, *104*, 331-340.

Camp, C. V. (2007). Design of space trusses using Big Bang–Big Crunch optimization. Journal of Structural Engineering, 133(7), 999-1008.

Carvalho, J. P., Lemonge, A. C., Hallak, P. H., & Vargas, D. E. (2018, September). A differential evolution to find the best material groupings in truss optimization. In *International Conference on Engineering Optimization* (pp. 102-114). Springer, Cham.

Chan, C. M., & Grierson, D. E. (1993). An efficient resizing technique for the design of tall steel buildings subject to multiple drift constraints. The Structural Design of Tall and Special Buildings, 2(1), 17-32.

Chan, C. M., & Chui, J. K. L. (2006). Wind-induced response and serviceability design optimization of tall steel buildings. *Engineering Structures*, *28*(4), 503-513.

Eberhart, R. C., & Kennedy, J. (1995, October). A new optimizer using particle swarm theory. In Proceedings of the sixth international symposium on micro machine and human science (Vol. 1, pp. 39-43).

Erol, O. K., & Eksin, I. (2006). A new optimization method: big bang–big crunch. Advances in Engineering Software, 37(2), 106-111.

Fernández-Cabán, P. L., & Masters, F. J. (2018). Hybridizing particle swarm and big bang-big crunch optimization methods to explore then exploit the design domain of large planar frame structures. *Computers & Structures*, *202*, 1-14.

Galante, M. (1996). Genetic algorithms as an approach to optimize real-world trusses. International Journal for Numerical Methods in Engineering, 39(3), 361-382.

Grierson, D. E., & Cameron, G. E. (1987). SODA-structural optimization design and analysis. Waterloo, Ontario, Canada: Waterloo Engineering Software.

Hasançebi, O. Ğ. U. Z. H. A. N., & Kazemzadeh Azad, S. (2014). Discrete size optimization of steel trusses using a refined big bang–big crunch algorithm. *Engineering Optimization*, *46*(1), 61-83.

Hasançebi, O., Bahçecioğlu, T., Kurç, Ö., & Saka, M. P. (2011). Optimum design of high-rise steel buildings using an evolution strategy integrated parallel algorithm. Computers & Structures, 89(21), 2037-2051.

Kashani, A. R., Camp, C. V., Rostamian, M., Azizi, K., & Gandomi, A. H. (2021). Population-based optimization in structural engineering: a review. Artificial Intelligence Review, 1-108.

Kaveh, A. (2021). Optimal Design of Large-Scale Frame Structures. In *Advances in Metaheuristic Algorithms for Optimal Design of Structures* (pp. 593-624). Springer, Cham.

Kaveh, A., & BolandGerami, A. (2017). Optimal design of large-scale space steel frames using cascade enhanced colliding body optimization. *Structural and Multidisciplinary Optimization*, *55*(1), 237-256.

Kaveh, A., & Talatahari, S. (2010). A discrete big bang-big crunch algorithm for optimal design of skeletal structures. Asian Journal of Civil Engineering, 11(1), 103-122.

Lemonge, A. C., Barbosa, H. J., Coutinho, A. L., & Borges, C. C. (2011). Multiple cardinality constraints and automatic member grouping in the optimal design of steel framed structures. *Engineering Structures*, *33*(2), 433-444.

Peng, B., Flager, F., Barg, S., & Fischer, M. (2021). Cost-based optimization of steel frame member sizing and connection type using dimension increasing search. *Optimization and Engineering*, 1-34.

Saka, M. P., & Geem, Z. W. (2013). Mathematical and metaheuristic applications in design optimization of steel frame structures: an extensive review. Mathematical problems in engineering, 2013.

Shea, K., Cagan, J., & Fenves, S. J. (1997). A shape annealing approach to optimal truss design with dynamic grouping of members.

Spence, S. M., & Kareem, A. (2014). Performance-based design and optimization of uncertain wind-excited dynamic building systems. *Engineering Structures*, *78*, 133-144.

Toğan, V., & Daloğlu, A. T. (2008). An improved genetic algorithm with initial population strategy and self-adaptive member grouping. *Computers & Structures*, *86*(11-12), 1204-1218.

Walls, R., & Elvin, A. (2010a). An algorithm for grouping members in a structure. *Engineering Structures*, *32*(6), 1760-1768.

Walls, R., & Elvin, A. (2010b). Optimizing structures subject to multiple deflection constraints and load cases using the principle of virtual work. Journal of Structural Engineering, 136(11), 1444-1452.